DOI: 10.1002/ejic.200701175

# Complex Effect of Partial Substitution of $La^{3+}$ by $Ca^{2+}$ on the Stability of Fast Oxide-Ion Conductor $La_2Mo_2O_9$

**Ania Selmi,[a] Gwenaël Corbel,[a] Stéphanie Kojikian,[a] Valentina Voronkova,[b] Elena Kharitonova,[b] and Philippe Lacorre*[a]**

**Keywords:** Ceramics / Phase transitions / Reversible demixing / Metastability / Temperature-controlled X-ray diffraction

Demixing/recombination and metastability phenomena are observed in the $La_{2-2x}Ca_{2x}Mo_2O_{9-x}$ solid solutions of LAMOX-type fast oxide-ion conductors ($0.005 \leq x \leq 0.05$). The demixing process is more visible at high Ca content. The effects of composition, sample shape (powders with two degrees of fineness, ceramic pellets, single crystals) and thermal history are studied by using high-temperature X-ray diffraction, differential scanning calorimetry (DSC) and polarized microscopy. All these parameters are shown to have an influence on the stability of, and transformations between, the ordered α and the disordered β forms of the LAMOX compounds. Powder samples with low Ca content ($x = 0.01$, 0.02) have been stabilized in the α form, and powder samples with higher Ca content ($x = 0.03$, 0.04, 0.05) are in the β form. Upon heating, the low-Ca-content compounds ($x = 0.01$ and $x = 0.02$) exhibit the α/β transition, whereas those with higher Ca content ($x = 0.03$ and $x = 0.04$) show a succession of β/α/β phase transformations (metastability of the β form). The compound with the highest Ca content ($x = 0.05$) remains in the β form over the whole thermal range. Upon cooling, all samples exhibit the β/α phase transition. When $x = 0.04$, powder annealing suppresses all the phase transformations upon heating, but not the β/α transition upon cooling, whereas sample shaping/sintering as a pellet stabilizes the β form over the whole thermal range upon heating and cooling. Single crystals with compositions $x = 0.005$ and $x = 0.025$ can be obtained either in the α or in the β form by slow cooling or by quenching, respectively. In these oxide-ion conductors with a high concentration of point defects, internal or external stress appears to strongly affect the vacancy equilibrium but not the demixing/recombination phenomenon.



## Introduction

The most commonly used electrolyte in solid oxide fuel cells (SOFCs) is currently yttrium-stabilized zirconia (YSZ), with working temperatures around 900 °C. Much effort is devoted to find alternative electrolyte materials with better conducting properties, which would therefore decrease the fuel cell working temperature.[1] In this context, the recent discovery of a new family of fast oxide-ion conductors (the so-called LAMOX family)[2] has attracted much interest, since its parent compound $La_2Mo_2O_9$ is a better oxide-ion conductor than the best known stabilized zirconia (8% YSZ) above 600 °C. As such, it could significantly lower the working temperature of SOFCs by about 150 °C. Even though $La_2Mo_2O_9$ undergoes an order/disorder phase transition around 580 °C from a monoclinic α phase to the highly cubic β phase,[3] with a concomitant abrupt volume change, most cationic substitutions tend to stabilize the highly conducting cubic β phase down to room temperature.[4] Recently, some work has been devoted to the study of the static/dynamic nature of oxide ions in $La_2Mo_2O_9$ by molecular dynamics simulations[5,6] and by atomic pair distribution function analysis.[7]

A drawback in the use of molybdates in SOFCs is the possibility that they will get reduced under low oxygen pressure. It has been previously shown that substitution of molybdenum by tungsten is likely to stabilize LAMOX compounds under reducing conditions.[8] Some of our studies have been devoted to the effect of isovalent substitutions of lanthanum or molybdenum on the properties of LAMOX compounds.[9,10] Other studies have focused on aliovalent substitutions, since they are a common way of tuning the vacancy concentration in order to enhance oxide-ion conductivity. One can cite, for instance, studies on the substitution of molybdenum by niobium or tantalum,[11] and of lanthanum by alkali[12] or alkaline earth metals.[13,14] In a previous paper,[15] some of us have presented the unusual instability phenomena observed in $La_{1.92}Ca_{0.08}Mo_2O_{8.96}$ (see Figure 1). In this compound, a demixing process occurs above 640 °C, in which calcium segregation out of the LAMOX phase leads to the formation of a $CaMoO_4$ impu-

[a] Laboratoire des Oxydes et Fluorures, UMR CNRS 6010, Université du Maine,
Avenue Olivier Messiaen, 72085 Le Mans cedex 9, France
E-mail: philippe.lacorre@univ-lemans.fr
[b] Faculty of Physics, M.V. Lomonosov Moscow State University, Leninskie Gory, Moscow 119992, Russia

Supporting information for this article is available on the WWW under http://www.eurjic.org or from the author.

  

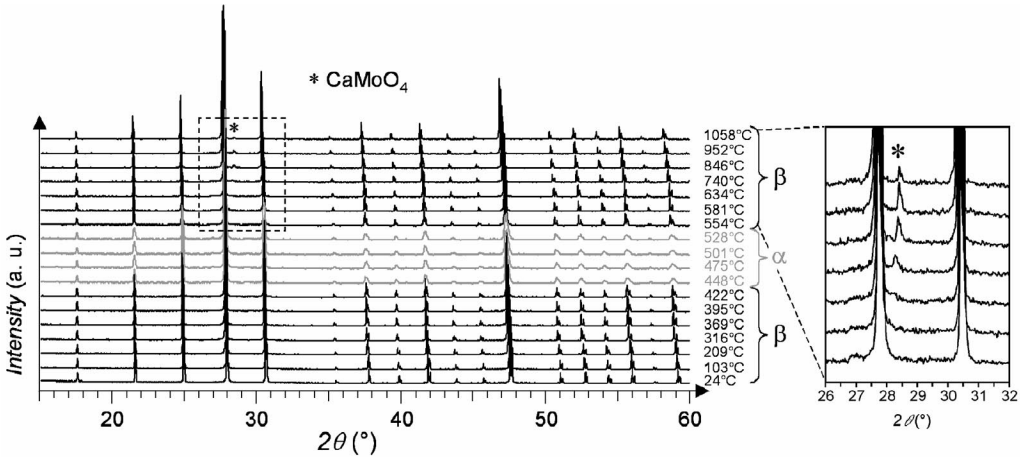


Figure 1. Temperature-controlled X-ray diffraction patterns, in the thermal range 24–1058 °C, of a 4 mol-% Ca powder sample prepared at 1150 °C, showing a succession of phase transformations. Right: enlargement of the $2\theta$ region and temperature range in which the $CaMoO_4$ main diffraction peak appears.

rity. At higher temperatures, a recombination process takes place which reforms the pure cubic LAMOX phase, thus allowing us to obtain the compound as a pure phase at room temperature through a relatively fast cooling rate of 5 °C/min. In addition, at lower temperatures, a metastability phenomenon of the β-type structure was observed by temperature-controlled X-ray powder diffraction on a powder sample, with double reversed β/α/β phase transition upon heating. However, in a pellet sample with the same composition, the β phase was shown to remain stable over the whole thermal range.

In the current paper, we extend the previous study to the $La_{2-2x}Ca_{2x}Mo_2O_{9-x}$ solid solution and investigate the effect of composition, thermal history, grain size and sample shaping/annealing (powders, ceramics, single crystals) on the complex sequence of events detected in the $x = 0.04$ sample. The succession of phase transformations has been studied in different types of samples by a variety of complementary methods in order to better understand the observed phenomena. In powder samples, DTA/DSC measurements helped us detect phase transitions and determine the effect of thermal cycling. Thermal X-ray diffraction allowed us to identify the nature of the phases involved in both powder and ceramic samples and to observe the phase transformation kinetics. Impedance spectroscopy was used to measure the effect of Ca substitution on conductivity in ceramic samples. The coexistence of two phases at the microscopic level was evidenced by TEM/HREM on powder samples and followed at high temperature by polarized light microscopy on single crystals. The results of these studies, devoted successively to powder samples, ceramic samples and single crystals, are presented in the next section.

## Results and Discussion

### Powder Samples

The XRD patterns of the $La_{2-2x}Ca_{2x}Mo_2O_{9-x}$ series show pure phases up to at least $x = 0.05$ (see Figure 2). The composition $x = 0.10$ is impure: it includes $CaMoO_4$ (scheelite-type structure). Subasri et al.[14] observed a substitution limit of $x = 0.04$. This slight discrepancy will be explained later on. Figure 2 shows that the $x = 0.04$ substitution stabilizes the cubic β phase at room temperature, whereas the $x = 0.01$ and $x = 0.02$ samples exhibit a monoclinic distortion demonstrated by the splitting of the (231) pseudocubic diffraction peak and the superstructure reflections observed around $2\theta = 26–27°$.[3] The $x = 0.03$ sample stabilizes a pseudo cubic β phase at room temperature with no superstructure reflections but diffraction peaks with a base wider than those of a standard cubic β phase like that of the $x = 0.04$ and $x = 0.05$ compounds.

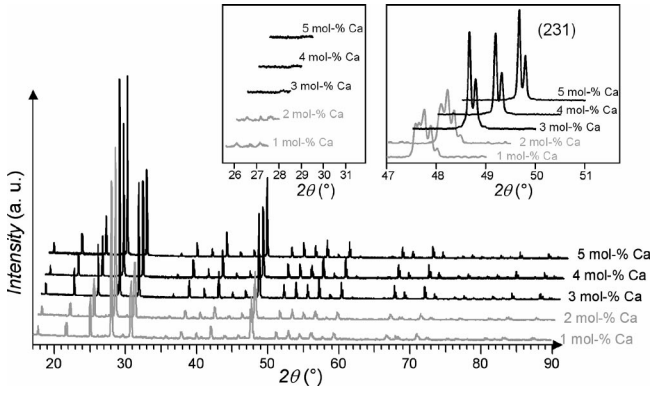


Figure 2. Room-temperature X-ray diffraction patterns of $La_{2-2x}Ca_{2x}Mo_2O_{9-x}$ for different Ca concentrations. Insets show $2\theta$ regions where the superstructure peaks (left) and monoclinic distortion (right) of the α form are visible.

DTA analyses confirm the observations made on the XRD patterns (see Figure S14 in the Supporting Information). Cyclic DSC measurements were carried out on the 4 mol-% Ca sample. The curves recorded during the heating stages in the 400–600 °C thermal range are presented in Figure 3. The endothermic peak around 454 °C exists on all curves, but its intensity decreases from cycle to cycle (Figure 3a). At higher temperatures, the other endothermic

  

peak characteristic of the α/β transition around 560 °C appears clearly in the second heating cycle only, and its intensity increases from cycle to cycle (Figure 3b).

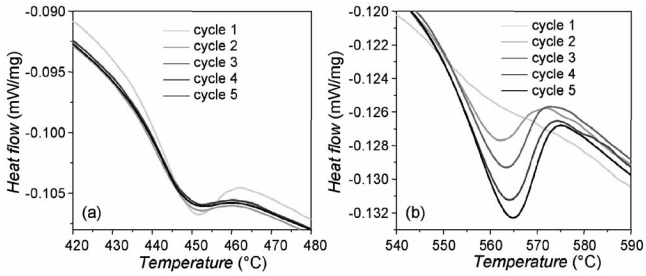


Figure 3. DSC measurements during the thermal cycling of a 4 mol-% Ca powder sample around 450 °C (a) and 560 °C (b) upon heating.

At higher temperature, above ca. 600–700 °C, the demixing process already observed in the 4 mol-% Ca sample occurs regardless of the Ca concentration. It is detectable through either a broadening of the diffraction peaks, due to Ca depletion (2 mol-% Ca, see Figure 4), or the appearance of a $CaMoO_4$ peak (3 mol-% Ca, 4 mol-% Ca, see Figure 1). No impurity peak is visible in the 2 mol-% Ca sample, because of the low amount of Ca in the solid solution. At higher Ca content, the absence or presence of peak splitting depends on the composition and on the duration of annealing, namely on whether Ca depletion is important enough to stabilize the distorted α form with low Ca content.

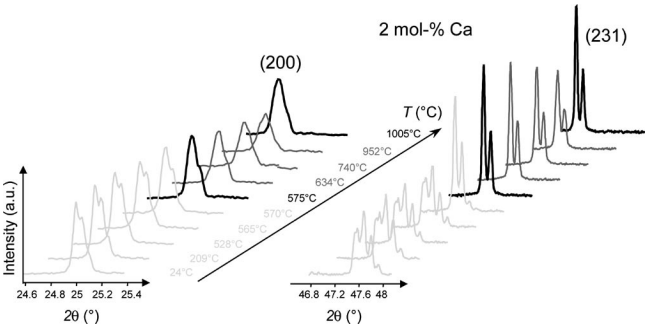


Figure 4. Temperature-controlled diffractograms of the (200) and (231) pseudocubic peaks of a 2 mol-% Ca powder sample, showing peaks splitting (low temperature, light grey) and widening (higher temperature, dark grey).

A problematic point in the preparation of the Ca-substituted series is the difficulty of obtaining pure phases, because of a narrow thermal stability range. The demixing/recombination phenomenon below the synthesis temperature is most certainly responsible for difficulties in determining the exact limit of the $(La,Ca)_2Mo_2O_{9-\delta}$ solid solution. When the sample is not prepared in the correct thermal range or is cooled down too slowly in the demixing thermal range, the $CaMoO_4$ impurity is likely to appear and remain present down to room temperature. For instance, it was said in a previous paper[14] that 4 mol-% Ca was the substitution limit, whereas we were able, by using appropriate thermal treatment, to prepare a pure 5 mol-% Ca sample. It might appear that, with proper synthesis conditions or at least in a certain thermal range, the substitution limit could be extended further.

Figure 5 shows the thermal evolution of the (pseudo)-cubic (231) reflection of the 2 mol-% Ca (a) and 3 mol-% Ca (b) samples upon heating up and of the 4 mol-% Ca (c) and 5 mol-% Ca (d) samples upon heating up and cooling down, under the conditions presented in the Experimental Section. This reflection is chosen, because it is the reflection that is split the most due to monoclinic distortion in $La_2Mo_2O_9$ (see inset in Figure 2). Whereas in the 2 mol-% Ca sample, a single α/β transition characteristic of the parent compound $La_2Mo_2O_9$ is apparent, the β/α/β double transition due to β phase metastability is present in both the 3 mol-% Ca and 4 mol-% Ca samples. In the 4 mol-% Ca sample, only one transformation is observed upon cooling down from the high-temperature β phase to the low-temperature α phase, with a small hysteresis relative to the process of heating up. This points out the metastable character of the low-temperature β phase. In comparison, the 5 mol-% Ca cubic sample (Figure 5d) shows no phase transformation upon heating up, whereas a transition to the low-temperature α phase is observed upon cooling down.

Figure 6 shows the phase stability and thermal evolution of cell volumes deduced from the high-temperature diffraction data for $x = 0.02$, $x = 0.03$ and $x = 0.04$. The stability domain of the α phase agrees well with the DTA study (see above). The cell volume of the α phase is generally smaller than that of the corresponding β phase.

At 422 °C, the low-temperature β/α (metastable/stable) phase transformation is rather slow (see Figure S15 in the Supporting Information). The reverse α/β phase transformation of the α form with the same composition has been followed by transmission electron microscopy. Figure 7a and Figure 7b show the electron diffraction patterns of the cubic β and monoclinic α phases, respectively, of the sample with 4 mol-% Ca composition. When the sample is observed in the high-resolution mode, the electron beam causes the monoclinic α ordered phase to transform into the cubic β disordered phase (see Figure 7c): the characteristic x2x4 superstructure of the monoclinic phase is visible on the top left part of the image, while the disordered cubic phase induced by the electron beam appears at the bottom-right (with the simulation in the inset). The electron diffraction pattern recorded after exposure to the high-resolution electron beam shows the almost complete disappearance of the superstructure spots (see Figure 7d).

## Ceramic Samples

Lubomirsky et al.[16] have pointed out that, in ionic conductors with a high concentration of point defects, application of an external stress could have a non-negligible influence on the defects equilibrium. Suspecting that sample shaping/sintering might have a similar effect on the order–disorder phase transitions of our LAMOX compounds, we have carried out several temperature-controlled diffraction

  

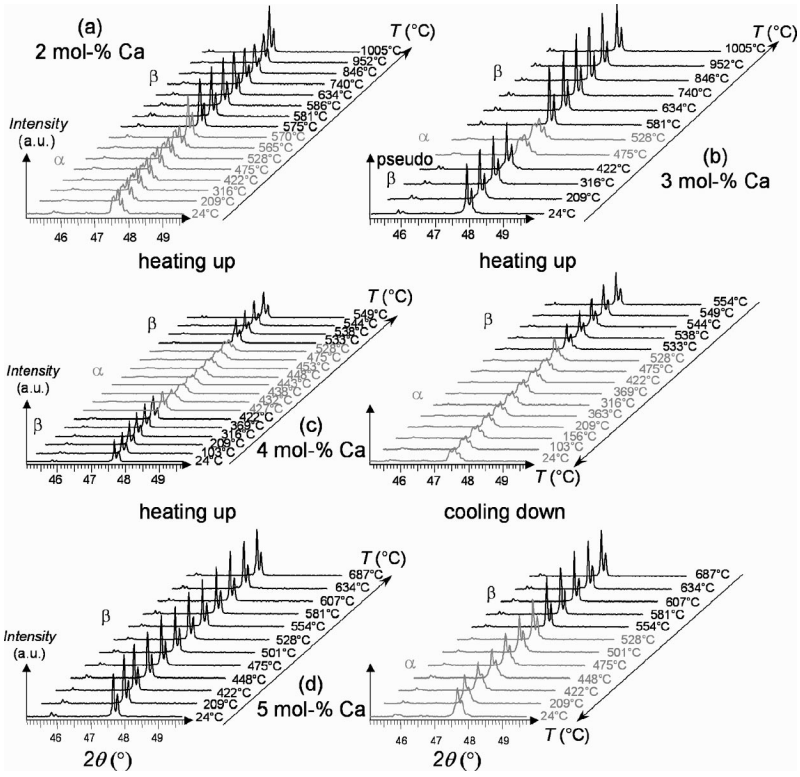


Figure 5. Temperature-controlled diffractograms of the (231) pseudocubic peak for powder samples of 2 mol-% Ca (a) and 3 mol-% Ca (b) upon heating (top), and of 4 mol-% Ca (c) and 5 mol-% Ca (d) upon heating (middle and bottom left) and cooling (middle and bottom right).

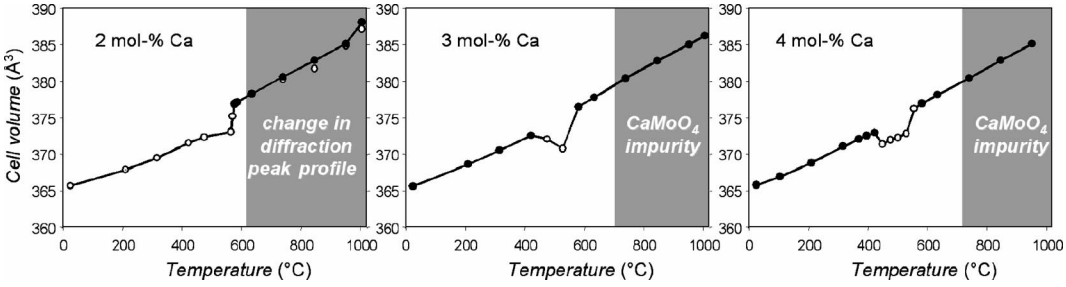


Figure 6. Thermal evolution of cell volume for 2 mol-% Ca, 3 mol-% Ca and 4 mol-% Ca powder samples (black points from Rietveld refinements in the cubic cell, open circles from Le Bail refinements in a single monoclinic cell). The grey areas indicate partial demixing.

studies on different kinds of samples with composition $La_{1.92}Ca_{0.08}Mo_2O_{8.96}$ (4 mol-% Ca). Three types of samples were prepared from a pure raw powder (sample 0) synthesized at 1150 °C according to the process defined in the Experimental Section: (a) the raw powder was ball-milled as described in the Experimental Section (conductivity measurements) to obtain sample 1; (b) sample 1 was annealed at 1200 °C for 4 h at a heating/cooling rate of 5 °C/min to obtain sample 2; (c) sample 1 was shaped as a pellet (13 mm diameter and ca. 0.5 mm thickness) with a drop of polyvinyl alcohol solution in a uniaxial press (ca. 0.15 GPa), then annealed at 300 °C for 5 h and finally sintered at 1200 °C for 4 h to yield sample 3.

The thermal evolution of the characteristic (231) reflection sensitive to monoclinic distortion was recorded upon heating up and cooling down, in the same conditions for the three samples. The corresponding XRD patterns are reported in Figure 8.

First of all, it can be observed that grinding has little effect on the phase stability, since the succession of phase transformations upon heating and cooling is the same for the raw (Figure 5c) and ground (Figure 8a) powders. However, when the ground powder is annealed at 1200 °C for 4 h (sample 2), a different behaviour is observed upon heating, since no more phase transition is observed, the sample remaining cubic over the whole thermal range (Figure 8b). It patently shows that high-temperature annealing has a direct effect on the relative stability of the α and β phases, since both samples, 1 and 2, have been obtained through the same cooling rate (5 °C/min). Nonetheless, the transition to a distorted monoclinic α phase is still observed upon cooling, as in the raw and ground samples. Note that the ther-

  

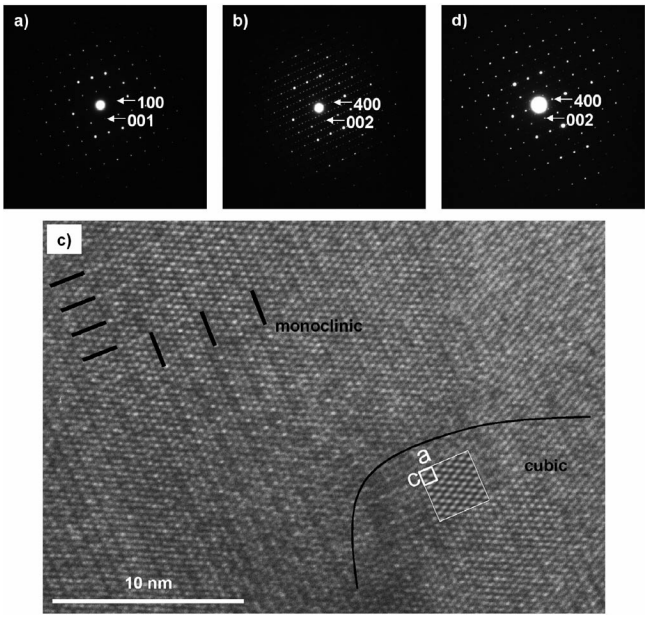


Figure 7. Transmission electron microscopy of 4 mol-% Ca samples: (a) selected area electron diffraction (SAED) of the cubic β phase along [010]; (b) SAED of the α phase along [010] before high-resolution electron microscopy (HREM); (c) HREM image along [010] of the previous sample, showing α phase (top-left) and β phase (bottom-right) domains; in the inset, simulated image of the β phase (thickness = 40 nm, defocus = –25 nm); (d) SAED along [010] of the previous sample after HREM.

mal behaviour of sample 2 is practically identical to that of the 5 mol-% Ca raw powder presented in Figure 5d.

Finally, when the ground sample is shaped in the form of a pellet and sintered at 1200 °C (sample 3), it does not exhibit any transition, either upon heating or upon cooling, and remains cubic over the whole studied thermal range (Figure 8c). This might result from the additional effect of the internal strain due to sample shaping (which is known to generate pressure gradients inside pellets)[17] and sintering. It is to be underlined here that the grinding/shaping/sintering process applied to the sample in order to make it dense and compact has a beneficial effect on the stabilization of the highly conducting β phase, which in this sample appears to be stable over the whole studied thermal range. This result was confirmed by a dilatometric study on another pellet sample, which did not show any trace of the β/α/β phase transitions (characterized by important changes in thermal expansion coefficient).

Concerning the global behaviour of the whole sample series, it can be observed that the phase stability of the ground sample annealed at 1200 °C (sample 2) is intermediate between those of the ground and pellet samples: similar to that of pellet sample 3 upon heating and to that of ground sample 1 upon cooling. It is also important to mention that, if the phase stability of Ca-substituted compounds is highly sensitive on shaping and thermal history, the demixing/recombination phenomenon evidenced earlier is not, since this phenomenon is observed in all samples.

In order to measure the influence of Ca substitution on ionic transport, we have carried out impedance spectroscopy measurements on the members of the $(La,Ca)_2Mo_2O_{9-\delta}$ series. This allowed us to detect the signature, on conductivity curves, of metastability and demixing phenomena. For instance, in Figure 9a are shown the conductivity curves of a 2 mol-% Ca pellet sample upon heating up and cooling down. Whereas a powder sample of the same composition exhibits the characteristic α/β transformation (see Figure 5a) observed in $La_2Mo_2O_9$, the conductivity curve for a pellet sample shows, upon heating, a conductivity plateau (or a decrease in conductivity relative to Arrhenius behaviour) in the thermal range 470–560 °C (hatched area in Figure 5a). It is likely that such a plateau is representative of the less conducting α phase, in between more conducting β phases at lower and higher temperatures. It gives an additional illustration of the (meta)stabilization of the β phase

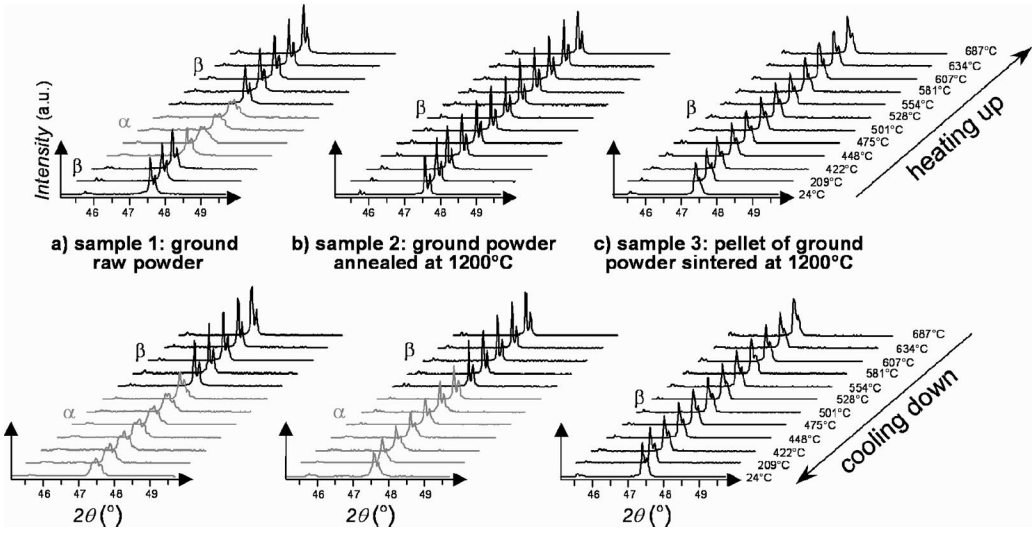


Figure 8. Temperature-controlled diffractograms of the pseudocubic peak (231) for 4 mol-% Ca samples with different grain size/shaping/sintering conditions during heating up (top) then cooling down (bottom).

  

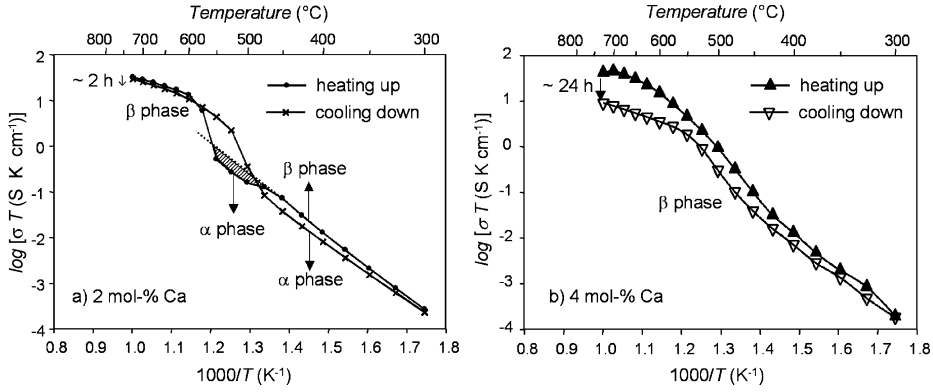


Figure 9. Conductivity curves of 2 mol-% Ca (a) and 4 mol-% Ca (b) pellet samples during heating up to 725 °C (with temperature maintained for 2 h and about 24 h, respectively) and cooling down. See text for comments.

by pellet shaping/sintering. Upon cooling down, the α phase is stabilized down to room temperature, with slightly lower conductivity than the metastable β phase below 470 °C.

In Figure 9b, an illustration is given of the effect of the demixing process on the conductivity of the 4 mol-% Ca sample. After being left for about 24 h at 725 °C in the conductivity measurement cell, a clear decrease in the conductivity of the sample is observed. This is due to the appearance of the resistive $CaMoO_4$ phase previously detected in our high-temperature XRD study. In order to have an unbiased appraisal of the effects of Ca substitution on LAMOX conductivity, we therefore have to keep to a temperature that is low enough to avoid demixing.

Contrary to the 2 mol-% Ca sample studied above, at lower temperature no abrupt change in conductivity is observed in the 4 mol-% Ca sample, as would be expected if β/α/β phase transformations would take place. This observation has been made on different pellet samples. It confirms the previous results on the total stabilization, for 4 mol-% Ca, of the β phase over the whole thermal range by pellet shaping/sintering. The departure from Arrhenius behaviour, observed in all cubic members of the LAMOX family, has previously been interpreted as possibly originating from a transition from static to dynamic disordering of oxygen vacancies (Arrhenius to Vogel–Tammann–Fulcher mechanisms).[5]

The effect of composition on the transport properties before demixing is shown in Figure 10. It shows that the progressive disappearance of the α phase results in a global increase in conductivity in the 450–580 °C range, but also that the substitution of $La^{3+}$ by $Ca^{2+}$ does not affect significantly the conductivity of the β phase. The conductivity of Ca-substituted β phases seems to remain lower than that of $La_2Mo_2O_9$ above 580 °C, and it does not exhibit any clear dependence on Ca content. This result is rather unexpected, since the substitution by an aliovalent cation modifies (in this case increases) the number of oxygen vacancies in the structure. However, this additional empty volume (see Figure S16 in the Supporting Information) cannot be considered as a "free volume" available for oxide ions to move, since the conductivity does not increase with Ca content. A possible explanation for such behaviour is vacancy trapping around calcium ions. Note also that the propensity to cationic segregation might result, even before demixing, in calcium clustering within the LAMOX phase, which could also be detrimental to conductivity.

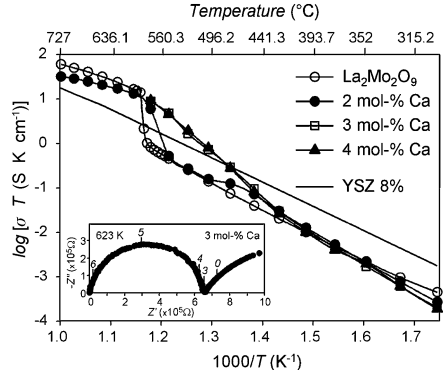


Figure 10. Conductivity curves (Arrhenius plots) of $La_{2-2x}Ca_{2x}Mo_2O_{9-x}$ for different Ca concentrations in comparison with that of 8% yttria stabilized zirconia (8% YSZ, courtesy of J. T. S. Irvine). Inset: complex impedance spectrum (Nyquist representation) of the 3 mol-% Ca sample at 623 K.

## Single Crystals

Ca-substituted single crystals (0.5 mol-% Ca and 2.5 mol-% Ca) were investigated by polarized microscopy and DSC methods. A previous study on $La_2Mo_2O_9$ single crystals showed that single crystals of the α-$La_2Mo_2O_9$ form with domains and of the β form can be obtained by slow cooling and by quenching from high temperature, respectively.[18] Piezoelectric tests[18] and nonlinear optical properties studied by SHG (second harmonic generation) powder measurements[10] demonstrated the polarity of α-$La_2Mo_2O_9$ crystals and suggested that the origin of domains in the crystals might be connected with their ferroelectricity. It is worth noting that domains are typical features of the monoclinic phase.

The Ca-substituted crystals quenched at room temperature were transparent and isotropic in polarized light (cubic

  

β phase in metastable state), whereas the slowly cooled crystals (< 1 °C/min) were in the anisotropic monoclinic α phase. All quenched cubic crystals annealed at 450 °C for 2 h transform into the anisotropic monoclinic α phase with appearance of ferroelectric domains. A sketch of phase stability during the heating and cooling processes of quenched and slowly cooled crystals is shown in Figure 11. At a cooling rate of 10 °C/min in the last step, in both cases, two phases are observed in the crystals (α and metastable β). This rate is not slow enough to generate the α phase only, which is stable at room temperature. Therefore the point at which two phases coexist in $La_{2-2x}Ca_{2x}Mo_2O_{9-x}$ single crystals cooled at a higher rate than 1 °C/min needs to be taken into account in studies of their physical properties, especially at room temperature.

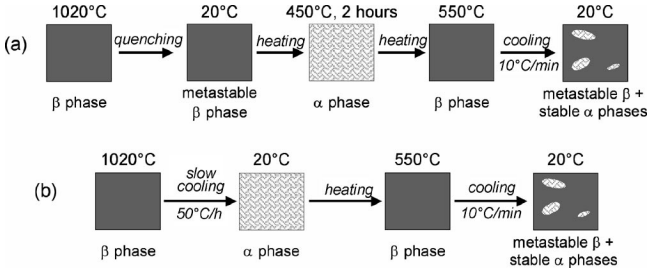


Figure 11. Sketch of heating and cooling processes of quenched (a) and slowly cooled (b) $La_{2-2x}Ca_{2x}Mo_2O_{9-x}$ crystals.

In Figure 12 the DSC data measured for $La_2Mo_2O_9$, $La_{1.99}Ca_{0.01}Mo_2O_{8.995}$ and $La_{1.95}Ca_{0.05}Mo_2O_{8.975}$ single crystals are shown. Wide endothermic peaks are observed in all crystals around 450 °C and 550 °C. The last event is connected with the ordinary α/β transition. The peak around 450 °C is appropriately ascribed to the transition from the metastable β phase to the monoclinic α phase, as observed when quenched crystals are annealed (Figure 11).

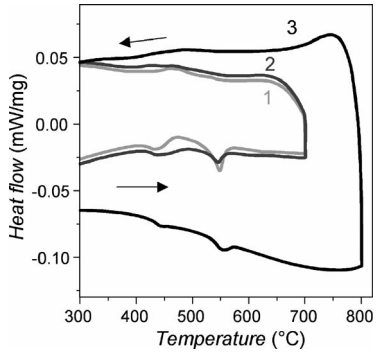


Figure 12. Scanning thermal analysis (STA) data for $La_2Mo_2O_9$ (1), 0.5 mol-% Ca (2) and 2.5 mol-% Ca (3) single crystals.

## Concluding Remarks

The temperature-controlled X-ray diffraction study of Ca-substituted $La_2Mo_2O_9$ fast oxide-ion conductors revealed an intricate behaviour with successive reversed phase transitions and/or demixing/recombination phenomena. The most complex process observed in this solid solution showed a succession of phases, where the β phase appears in three independent thermal domains (see Figure 13).

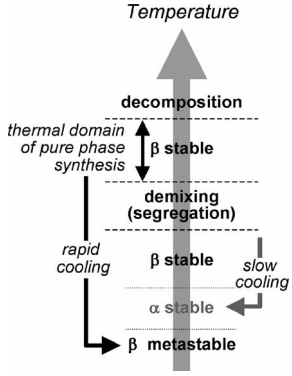


Figure 13. Complex succession of phases observed when heating up and cooling down 3 mol-% Ca and 4 mol-% Ca powder samples.

The complexity of the oxide-ion order in the α phase structure[19] makes possible the existence of the β phase at room temperature as a metastable phase. Many factors such as the synthesis temperature, the cooling and heating rates, the nature of the substituting element and sample shaping/sintering have an influence on its freezing. The added energy of annealing at temperatures near 450 °C is necessary to turn the sample into the stable state. Substituents and different thermal treatments can hard lock the β/α transition. This is confirmed by X-ray data on powders and by single-crystal investigations. Heating–cooling cycling results in a change in the high-temperature thermal signal intensity (Figure 3), thus suggesting a variation in the oxygen/vacancy distribution. A similar dependence of the high-temperature α/β phase transition on the thermal history of the sample had already been observed in $La_2Mo_2O_9$ by Hayward and Redfern.[20] It does not explain, however, in our case, the small variation in the intensity of the β/α low-temperature thermal signal.

In our substituted compounds with demixing/recombination processes, the thermal domain in which the pure phase can be synthesized is rather narrow, which can explain the difficulty to determine precisely the compositional limit of the solid solution.[13] In order to fully understand the demixing/recombination process observed in these compounds, more work is needed, for instance, along the line defined in ref.[21] for the study of segregation processes observed in ceramic materials during cooling. Such processes are likely to compete with oxide-ion/vacancy mobility and affect the conductivity properties.

If sample grinding, annealing or pressing/shaping do not affect the demixing process detrimental to oxide-ion conductivity above 600 °C, they have a clear impact on the disordered β phase stability below this temperature: ground powders do not behave in the same way as compact pellets. Such a difference in behaviour does not appear to originate from the grain size, since samples with close compositions but different grain sizes exhibit the same kind of phase

  

transformations. For instance, the 3 mol-% Ca and 4 mol-% Ca raw powder samples and the 4 mol-% Ca ground powder sample show the same β/α/β transitions upon heating (Figure 5b, c). Moreover, the DTA data for the 2.5 mol-% Ca single crystals (see Figure 12) show thermal peaks characteristic of the β/α and α/β transitions in the same temperature ranges as the same transformations observed by temperature-controlled XRD on the powder sample with a close 3 mol-% Ca composition (Figure 5b). Therefore, in the 2.5–4 mol-% Ca composition range, all samples with disaggregated particles, whose size ranges from micrometre (ground milled powder) to millimetre (single crystals), exhibit the β/α/β phase transitions. In comparison, when the 4 mol-% Ca samples are sintered, in the form of either aggregated powders or dense ceramics, the β/α/β transitions disappear, and the β form remains stable upon heating. This clearly suggests that external and/or internal strain due to the pressing and/or sintering processes have a direct incidence on the phase stability, hence on the oxygen/vacancy equilibrium state. This phenomenon has already been somewhat foreshadowed by Tarancón et al. in $La_2Mo_2O_9$ itself[22] and recently evidenced in other fast oxide-ion conductors with a high concentration of point defects.[15]

Finally this study has shown that, in these materials, the delicate balance in the anion/vacancy and cation/cation distributions is greatly affected by numerous factors, among which are thermal history, chemical composition or mechanical stress. These results are of particular interest not only for the fundamental understanding of the behaviour of ionic conductors, but also for practical purposes, since they might open up ways to more efficiently optimize their properties by appropriate thermal treatment and/or sample shaping. Generally, stability problems are underestimated in most studies devoted to solid electrolytes. The optimization of anionic conductivity usually relies on aliovalent cationic substitutions. However, in these compounds, high oxide-ion/vacancy diffusion considerably weakens the cationic network and makes it vulnerable to cation migration, even in the absence of an electric field and prior to any reaction with electrode materials. For instance, even in what is considered as the standard stable solid oxide electrolyte YSZ, substantial yttrium segregation is observed simply upon cooling down the sample.[23] Therefore, the effects we observe in the Ca-LAMOX family should not be considered as specific to this family of compounds. However, if, under certain conditions, they appear to be enhanced in this family, this provides the opportunity to better characterize, then understand and control these phenomena.

## Experimental Section

**Synthesis:** The $La_{2-2x}Ca_{2x}Mo_2O_{9-x}$ series ($x$ = 0.01, 0.02, 0.03, 0.04, 0.05, 0.10) was prepared by conventional solid-state reaction. Reactant powders ($CaCO_3$ and $La_2O_3$ preheated at 100 and 1000 °C, respectively, and $MoO_3$) were stoichiometrically weighted, ground and at first heated at 500 °C for 12 h in an alumina crucible. After several intermediate stages of heating and regrinding, pure samples were obtained after a final firing at 1100 °C ($x$ = 0.01, 0.02, 0.03) and 1150 °C ($x$ = 0.04, 0.05), which were then cooled down to room temperature at 5 °C/min. The $x$ = 0.1 sample was not pure after firing at 1200 °C. The $La_2Mo_2O_9$ and $La_{2-2x}Ca_{2x}Mo_2O_{9-x}$ millimetre-size single crystals studied were grown by means of spontaneous nucleation from flux in the $La_2O_3$–$MoO_3$ and $La_2O_3$–$MoO_3$–CaO systems. A mixture containing chemically pure 29 mol-% $La_2O_3$ and 71 mol-% $MoO_3$ and two mixtures with addition of 2 or 6 mol-% $CaCO_3$ were heated up to 1200 °C in alumina crucibles. The melts were homogenized at this temperature for a day and then cooled to 1020 °C at a rate of 1 °C/h. The residual melts were poured off, and crucibles with grown crystals were cooled down to room temperature at a rate of 50 °C/h or by quenching in air. The crystals were then mechanically extracted from the residual solvent. The crystal composition was determined by a Comebax SX-50 microanalyzer. The crystals obtained in this way had the composition $La_{1.99}Ca_{0.01}Mo_2O_{8.995}$ (0.5 mol-% Ca) and $La_{1.95}Ca_{0.05}Mo_2O_{8.975}$ (2.5 mol-% Ca).

**Structural Characterization:** A $\theta/\theta$ Bragg–Brentano Philips X′pert MPD PRO diffractometer (Cu-$K_{\alpha 1+2}$ radiations) equipped with the X′celerator detector was used to record XRD patterns of powders and sintered pellets at and above room temperature. Room-temperature diffractograms were collected in the 15–130° scattering-angle range for 207 min with a 0.0167° step. The Rietveld program FullProf was used for full-pattern matching.[24] The same diffractometer equipped with a HTK 1200 Anton Paar chamber was used to record diffractograms at given temperatures (see the thermal calibration in ref.[25]) between 24 and 1060 °C in the 9–130° range over 197 min with a 0.0167° step. A thermal stabilization time of 20 min was used before each scan, and the heating rate between two thermal steps was 10 °C/min. The temperature-controlled diffraction study of the (231) reflection of the $x$ = 0.04 sample consisted of recording for 11 min this reflection upon heating from 24° to 687 °C and cooling back to 24 °C (scattering-angle range: 45–50°, step 0.0167°, temperature stabilization: 20 min, heating rate: 10 °C/min). A study of phase-transition kinetics was also carried out on the latter compound by heating to 400 °C (heating rate: 10 °C/min, temperature stabilization: 20 min) and recording 195 diffractograms at this temperature, for 640 s each, in the 46.9–48.1° scattering-angle range with a 0.0167° step. The electron microscopy study (both electron diffraction and high-resolution imaging) was performed with a 200 kV JEOL 2010 TEM equipped with a side-entry, ±30° double tilt specimen holder. The powder was ground in absolute ethanol and spread over a holey carbon grid. Image simulation has been carried out with the EMS software package.[26]

**Thermal Analyses:** Differential thermal analyses (DTA) were performed under air flow in the temperature range 25–650 °C with a heating/cooling rate of 20 °C/min, on 25–29 mg samples in Pt crucibles by using a TGA/DSC Q600 SDT TA Instruments apparatus. Alumina powder was used as a reference. Differential scanning calorimetry (DSC) and scanning thermal analysis (STA) were performed for crystals (0.3–1 mm) and for powder samples by using NETZSCH DSC 204 F1 (30–590 °C, 10 °C/min, Al crucibles) and NETZSCH STA 449 C (30–800 °C, 10 °C/min, $Al_2O_3$ crucibles) equipment on 50–150 mg samples with 3–5 cycles of heating–cooling for each sample. An empty crucible was used as a reference.

**Conductivity Measurements**: All samples were ball-milled (FRITSCH Planetary micro mill Pulverisette apparatus with 900 mg of sample, in agate vials together with six agate balls 12 mm in diameter, in ethanol) for 4 alternations of 15-min milling sequences at 700 rpm, with a 15-min pause in between. The obtained ground powder samples were then shaped as pellets by using a uni-

  

axial press at first. They were then pressed at room temperature in an isostatic Top Industrie press under about 0.5 GPa and eventually sintered at 1100 °C for 12 h ($x$ = 0.01, 0.02, 0.03) and at 1200 °C for 4 h ($x$ = 0.04) with a heating/cooling rate of 5 °C/min. By this method, pellets (ca. 4.3 mm diameter and 2.5–2.8 mm thickness) were obtained with a relative density of about 96% of the theoretical absolute value calculated from X-ray diffraction data. Thin platinum films deposited by RF sputtering on both faces of the pellet samples were used as electrodes. The impedance spectra were collected in flow-dried air in a Schlumberger Solartron SI 1260 frequency response analyzer working with Dielectric Interface Solartron 1296 in the frequency range 0.05 Hz to 10 MHz. Each data point was recorded at an AC voltage of 0.05 V after 30 min of thermal stabilization in dried air. The Z-view 2.7 software was used to analyze the impedance data and determine the resistance of the ceramic pellets.

**Supporting Information** (see also the footnote on the first page of this article): The Supporting Information file includes colour versions of the paper figures (S1–S13), together with three supplementary figures, S14, S15 and S16. Figure S14 presents DTA measurements of $La_{2-2x}Ca_{2x}Mo_2O_{9-x}$ powder samples for different Ca concentrations. XRD data recorded at 422 °C show the slow β/α phase transition in a 4 mol-% Ca powder sample in Figure S15. Figure S16 shows the evolution with Ca content of the cell volume and of the fraction of unoccupied volume.

## Acknowledgments

The Pays-de-la-Loire Region is acknowledged for its participation in the funding of A. Selmi's thesis grant. E. Kharitinova and V. Voronkova would like to thank the Russian Foundation for Basic Research for the financial support (grant 07-02-00180)

[1] V. V. Kharton, F. M. B. Marques, A. Atkinson, *Solid State Ionics* **2004**, *174*, 135–149.
[2] P. Lacorre, F. Goutenoire, O. Bohnke, R. Retoux, Y. Laligant, *Nature* **2000**, *404*, 856–858.
[3] F. Goutenoire, O. Isnard, R. Retoux, P. Lacorre, *Chem. Mater.* **2000**, *12*, 2575–2580; P. Lacorre, F. Goutenoire, F. Altorfer, D. Sheptyakov, F. Fauth, E. Suard, *Adv. Sci. Technol.* **2003**, *33*, 737–747.
[4] F. Goutenoire, O. Isnard, E. Suard, O. Bohnke, Y. Laligant, R. Retoux, P. Lacorre, *J. Mater. Chem.* **2001**, *11*, 119–124.
[5] P. Lacorre, A. Selmi, G. Corbel, B. Boulard, *Inorg. Chem.* **2006**, *45*, 627–635.
[6] C. J. Hou, Y. D. Li, P. J. Wang, C. S. Liu, X. P. Wang, Q. F. Fang, D. Y. Sun, *Phys. Rev. B* **2007**, *76*, 014104.
[7] L. Malavasi, H. Kim, S. J. L. Billinge, T. Proffen, C. Tealdi, G. Flor, *J. Am. Chem. Soc.* **2007**, *129*, 6903–6907.
[8] S. Georges, F. Goutenoire, Y. Laligant, P. Lacorre, *J. Mater. Chem.* **2003**, *13*, 2317–2321.
[9] S. Georges, F. Goutenoire, F. Altorfer, D. Sheptyakov, F. Fauth, E. Suard, P. Lacorre, *Solid State Ionics* **2003**, *161*, 231–241.
[10] G. Corbel, Y. Laligant, F. Goutenoire, E. Suard, P. Lacorre, *Chem. Mater.* **2005**, *17*, 4678–4684.
[11] Z. S. Khadasheva, N. U. Venskovskii, M. G. Safronenko, A. V. Mosunov, E. D. Politova, S. Yu. Stefanovich, *Inorg. Mater.* **2002**, *38*, 1168–1171; S. Basu, P. Sujatha Devi, H. S. Maiti, *J. Electrochem. Soc.* **2005**, *152*, A2143–A2147.
[12] C. Tealdi, G. Chiodelli, L. Malavasi, G. Flor, *J. Mater. Chem.* **2004**, *14*, 3553–3557; X. P. Wang, Z. J. Cheng, Q. F. Fang, *Solid State Ionics* **2005**, *176*, 761–765.
[13] X. P. Wang, Q. F. Fang, *Solid State Ionics* **2002**, *146*, 185–193; S. Basu, P. Sujatha Devi, H. S. Maiti, *Appl. Phys. Lett.* **2004**, *85*, 3486–3488; T. He, Y. Huang, Q. He, Y. Ji, L. Pei, J. Liu, Z. Lu, *J. Alloys Compd.* **2005**, *388*, 145–152.
[14] R. Subasri, D. Matusch, H. Näfe, F. Aldinger, *J. Eur. Ceram. Soc.* **2004**, *24*, 129–137.
[15] A. Selmi, G. Corbel, P. Lacorre, *Solid State Ionics* **2006**, *77*, 3051–3055.
[16] I. Lubomirsky, *Solid State Ionics* **2006**, *177*, 1639–1642; M. Greenberg, E. Wachtel, I. Lubomirsky, J. Fleig, J. Maier, *Adv. Funct. Mater.* **2006**, *16*, 48–52.
[17] I. Yu. Prokhorov, *J. Eur. Ceram. Soc.* **1999**, *19*, 2619–2623.
[18] V. I. Voronkova, V. K. Yanovski, E. P. Kharitonova, *Crystallogr. Rep.* **2005**, *50*, 874–876.
[19] I. Evans, Yu. Howard, J. Evans, *Chem. Mater.* **2005**, *17*, 4074–4077.
[20] S. A. Hayward, S. A. T. Redfern, *J. Phys.: Condens. Matter* **2004**, *16*, 3571–3583.
[21] G. Petot-Ervas, C. Petot, *J. Eur. Ceram. Soc.* **1990**, *6*, 323–330; C. Petot, G. Petot-Ervas, M. Tebtoub, J. W. Fraser, M. J. Graham, G. I. Sproule, *Solid State Ionics* **1997**, *95*, 65–72.
[22] A. Tarancón, T. Norby, G. Dezanneau, A. Morata, F. Peiró, J. R. Morante, *Electrochem. Solid-State Lett.* **2004**, *7*, A373–A375.
[23] Y. Y. Lei, Y. Ito, N. D. Browning, T. J. Mazanec, *J. Am. Ceram. Soc.* **2002**, *85*, 2359–2363; M. Kilo, *Defect and Diffusion Forum* **2005**, *242–244*, 185–253; A. Rizea, G. Petot-Ervas, C. Petot, M. Abrudeanu, M. J. Graham, G. I. Sproule, *Solid State Ionics* **2007**, *177*, 3417–3424.
[24] J. Rodriguez-Carvajal, *Physica B* **1993**, *192*, 55–69.
[25] G. Corbel, S. Mestiri, P. Lacorre, *Solid State Sciences* **2005**, *7*, 1216–1224.
[26] P. Stadelmann, *Ultramicoscopy* **1987**, *21*, 131–145.

Received: October 31, 2007
Published Online: February 27, 2008

  